



# Constraining the Contribution of Hydrothermal Iron to Southern Ocean Export Production Using Deep Ocean Iron Observations

Alessandro Tagliabue<sup>1\*</sup>, Andrew R. Bowie<sup>2,3</sup>, Thomas Holmes<sup>2</sup>, Pauline Latour<sup>2</sup>, Pier van der Merwe<sup>2,3</sup>, Melanie Gault-Ringold<sup>3</sup>, Kathrin Wuttig<sup>3</sup> and Joseph A. Resing<sup>4</sup>

<sup>1</sup> School of Environmental Sciences, University of Liverpool, Liverpool, United Kingdom, <sup>2</sup> Institute for Marine and Antarctic Studies, University of Tasmania, Hobart, TAS, Australia, <sup>3</sup> Antarctic Climate and Ecosystems Cooperative Research Centre, Hobart, TAS, Australia, <sup>4</sup> NOAA Pacific Marine Environmental Laboratory, Cooperative Institute for Climate, Ocean, and Ecosystem Studies, University of Washington, Seattle, WA, United States

## OPEN ACCESS

### Edited by:

Sunil Kumar Singh,  
Physical Research Laboratory, India

### Reviewed by:

John Patrick Dunne,  
Geophysical Fluid Dynamics  
Laboratory (GFDL), United States  
Hajime Obata,  
The University of Tokyo, Japan  
Kazuhiro Misumi,  
Central Research Institute of Electric  
Power Industry (CRIEPI), Japan

### \*Correspondence:

Alessandro Tagliabue  
a.tagliabue@liverpool.ac.uk

### Specialty section:

This article was submitted to  
Marine Biogeochemistry,  
a section of the journal  
Frontiers in Marine Science

**Received:** 06 August 2021

**Accepted:** 19 January 2022

**Published:** 10 March 2022

### Citation:

Tagliabue A, Bowie AR, Holmes T,  
Latour P, van der Merwe P,  
Gault-Ringold M, Wuttig K and  
Resing JA (2022) Constraining  
the Contribution of Hydrothermal Iron  
to Southern Ocean Export Production  
Using Deep Ocean Iron Observations.  
*Front. Mar. Sci.* 9:754517.  
doi: 10.3389/fmars.2022.754517

Hydrothermal iron supply contributes to the Southern Ocean carbon cycle via the regulation of regional export production. However, as hydrothermal iron input estimates are coupled to helium, which are uncertain depending on whether helium inputs are based on ridge spreading rates or inverse modelling, questions remain regarding the magnitude of the export production impacts. A particular challenge is the limited observations of dissolved iron (dFe) supply from the abyssal Southern Ocean ridge system to directly assess different hydrothermal iron supply scenarios. We combine ocean biogeochemical modelling with new observations of dFe from the abyssal Southern Ocean to assess the impact of hydrothermal iron supply estimated from either ridge spreading rate or inverse helium modelling on Southern Ocean export production. The hydrothermal contribution to dFe in the upper 250 m reduces 4–5 fold when supply is based on inverse modelling, relative to those based on spreading rate, translating into a 36–73% reduction in the impact of hydrothermal iron on export production. However, only the spreading rate input scheme reproduces observed dFe anomalies > 1 nM around the circum-Antarctic ridge. The model correlation with observations drops 3 fold under the inverse modelling input scheme. The best dFe scenario has a residence time for hydrothermal iron that is between 21 and 34 years, highlighting the importance of rapid physical mixing to surface waters. Overall, because of its short residence time, hydrothermal Fe supplied locally by circum-Antarctic ridges is most important to the Southern Ocean carbon cycle and our results highlight decoupling between hydrothermal iron and helium supply.

**Keywords:** trace metals, hydrothermalism, Southern Ocean, biogeochemical modelling, iron cycle in oceans

## INTRODUCTION

The important role of hydrothermal iron (Fe) supply in shaping iron biogeochemical cycling has emerged over the last two decades (German et al., 2016; Tagliabue et al., 2017). In particular, hydrothermal Fe has been hypothesised to contribute to supporting the export production that supports the biological carbon pump in the Fe-limited Southern Ocean (Resing et al., 2015;

Tagliabue and Resing, 2016) and to act as a buffer against shorter term variations in other Fe sources (Tagliabue et al., 2010). To assess the large scale impact of hydrothermal Fe on the ocean carbon cycle, ocean models have coupled Fe and mantle helium-3 ( $^3\text{He}$ ) supply fluxes, which are known to vary according to ridge spreading rates (Farley et al., 1995; Dutay et al., 2004), using an assumed  $\text{Fe}/^3\text{He}$  ratio (Tagliabue et al., 2010). Hydrothermal Fe signals have been observed on or adjacent to ridge systems in all major ocean basins (Klunder et al., 2011, 2012; Nishioka et al., 2013; Saito et al., 2013; Rijkenberg et al., 2014; Hatta et al., 2015; Resing et al., 2015), but those in the Southern Ocean play the dominant role in shaping the impact on the biological carbon pump via changing export production (Tagliabue and Resing, 2016). Direct observations have shown hotspots of biological activity in the Southern Ocean linked to rapid upwelling of hydrothermal Fe from the south-west Indian ridge system (Ardyna et al., 2019) and in the south Pacific sector (Schine et al., 2021).

Inverse modelling efforts have led to a revision of the overall magnitude and spatial distribution of  $^3\text{He}$  supply in recent years, especially for Southern Ocean ridges. As part of the Ocean Carbon Model Intercomparison Project (OCMIP),  $^3\text{He}$  injection fields were created based on ridge spreading rate (Dutay et al., 2004) and are referred to here as “*spreading*” boundary forcing. Alternative estimates of  $^3\text{He}$  input are based on inverse modelling and do not make any *a priori* link between  $^3\text{He}$  supply and spreading rate, but instead optimise the distribution of He input along ridges using water column  $^3\text{He}$  measurements in a data-constrained ocean circulation inverse model (OCIM; DeVries and Holzer, 2019). This approach is referred to here as “*inverse*” boundary forcing. While the *spreading* and *inverse* forcings also differ in the magnitude of  $^3\text{He}$  supply (Dutay et al., 2004; DeVries and Holzer, 2019), most notable are the differences in the distribution of  $^3\text{He}$  supply along the global mid-ocean ridge crest. In particular, the *inverse* input has a strong reduction in He input from Southern Ocean ridges (DeVries and Holzer, 2019), compared to that from the *spreading* input scheme (Dutay et al., 2004; Bianchi et al., 2010; Holzer et al., 2017). Simple hydrothermal Fe model experiments using the *inverse*  $^3\text{He}$  input scenario suggest that hydrothermal Fe would have a short residence time and be largely trapped in the ocean interior with very little reaching the surface ocean (Roshan et al., 2020). This challenges the role of hydrothermal Fe in supporting export production and the regional biological carbon pump.

While linking  $^3\text{He}$  and hydrothermal Fe has been a useful way to fingerprint hydrothermal Fe anomalies in field datasets, their utility in driving a strict quantitative supply of hydrothermal Fe may be limited. The injection rates of mantle  $^3\text{He}$  have been assumed to be related to the spreading rate of ridges and an  $\text{Fe}/^3\text{He}$  ratio has been used to derive hydrothermal Fe input. However, compilation of prior datasets collected close to vents (Tagliabue et al., 2010), as well as consideration of vent-specific fluid end member signatures (Jenkins et al., 2015), have shown that a single  $\text{Fe}/^3\text{He}$  injection ratio is unlikely to be appropriate. Indeed, more detailed model-data comparisons have tended to find that the  $\text{Fe}/^3\text{He}$  ratio often needs local adjustment to match dFe observations (Tagliabue et al., 2010; Saito et al., 2013;

Resing et al., 2015; Roshan et al., 2020). At the spatial and temporal scales relevant for ocean models, the effective  $\text{Fe}/^3\text{He}$  ratio represents the integration of processes operating locally in the buoyant hydrothermal plume, as well as the factors that determine the longevity of hydrothermal Fe in the dispersing neutrally buoyant plume (German et al., 2016; Tagliabue and Resing, 2016). Field studies coupling dFe and  $^3\text{He}$  observations would provide constraints on these different processes, but where available, have been restricted to large scale GEOTRACES ocean sections that were not designed to track the Lagrangian evolution of hydrothermal plumes in time (Jenkins et al., 2018). Moreover, dFe data from the key Southern Ocean ridge systems remains very limited (Schlitzer et al., 2018), with most studies to date having little or no resolution in the abyssal ocean.

In this study, we test the influence of the *spreading* and *inverse*  $^3\text{He}$  input schemes on the distribution of dFe and carbon cycle using the NEMO-PISCES global ocean biogeochemical model. By combining these scenarios with new dFe observations across the circum-Antarctic ridge south of Tasmania (GEOTRACES GS01 section), we are able to appraise the likelihood of different scenarios for hydrothermal Fe input and their role in governing the regional carbon cycle.

## METHODS

The NEMO-PISCES model used here includes multiple limiting nutrients and a complex representation of the supply and cycling of Fe and a complete marine carbon cycle (Aumont et al., 2015). This version includes the dynamic representation of iron binding ligands and accounts for loss of organic Fe via coagulation and free Fe via particle scavenging (Völker and Tagliabue, 2015). The source of ligands from hydrothermal vents is set to 0.5 times the dFe supply rate. The control version of the model is run with no hydrothermal Fe input and only dust, sedimentary and riverine dFe supply. We then ran two hydrothermal scenarios using the *spreading* and *inverse* helium boundary forcing fields as a basis for the supply of hydrothermal Fe. The *spreading* experiment, used in prior studies, has 1,000 moles of  $^3\text{He}$  input per year and a  $\text{Fe}/^3\text{He}$  ratio of  $10 \times 10^6$  mol/mol, which equates to a total hydrothermal Fe input of  $10 \times 10^9$  mol/yr. The *inverse* experiment [based on the “CTL” experiment of DeVries and Holzer (2019)] has 600 moles of  $^3\text{He}$  input per year. For the *inverse* experiment, we used a higher  $\text{Fe}/^3\text{He}$  ratio of  $17 \times 10^6$  mol/mol to ensure a roughly identical total hydrothermal Fe supply. In this way, we test the consequences of the altered spatial distribution rather than total hydrothermal Fe input. A final experiment designed to test alternative estimates of hydrothermal Fe supply, combines the  $\text{Fe}/^3\text{He}$  ratio of  $6.4 \times 10^6$  mol/mol optimised by Roshan et al. (2020) with the *inverse*  $^3\text{He}$  input field (to yield a total hydrothermal iron supply of  $3.8 \times 10^9$  mol/yr) and is referred to as “*inverseR*.” All model runs were integrated for 500 years.

The SR3 repeat hydrographic line south of Tasmania to Antarctica (along  $\sim 140^\circ\text{E}$ ) was re-occupied in austral summer of 2018, and a full-depth GEOTRACES section (GS01) completed, including 51 deployments of an autonomous 12-bottle trace metal clean rosette system. Sampling and analysis for iron and

other trace metals followed procedures as described previously (Wuttig et al., 2019) with a limit of detection of 0.03–0.05 nmol kg<sup>-1</sup>. The SR3 section crosses the south east Indian Ridge south of Australia between approximately 52 and 56°S.

## RESULTS AND DISCUSSION

### Impact of Hydrothermal Fe Supply Scenarios on Iron Cycling

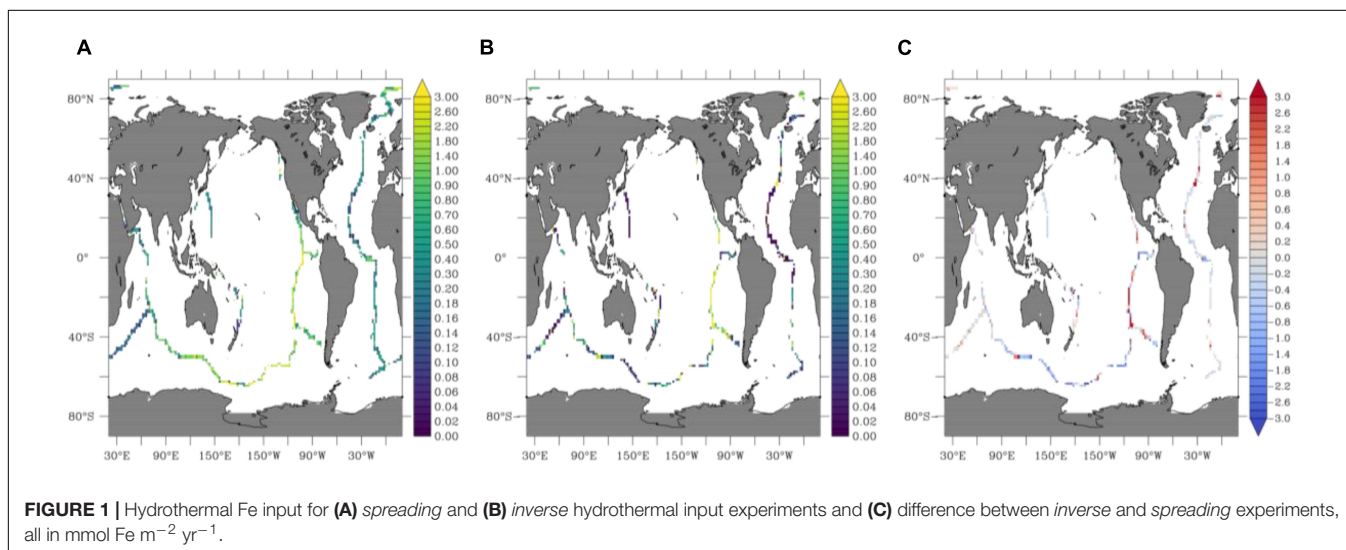
The hydrothermal Fe supply from the *spreading* experiment follows the ridge spreading rate variability and the *inverse* experiment increases <sup>3</sup>He and Fe input from the South East Pacific Rise (SEPR) in particular, while decreasing it along Southern Ocean ridges [Figure 1, as reported previously (DeVries and Holzer, 2019; Roshan et al., 2020)]. In the *inverse* experiment, the SEPR dominates regional hydrothermal Fe input, aside from a few, localised hotspots along other ridge systems (Figures 1B,C). We cannot closely examine the inferred <sup>3</sup>He injection rates north of the equator in the Atlantic Ocean from the *inverse* experiment, due to the exclusion of <sup>3</sup>He observations from the inverse modelling procedure in this region due to contamination from tritium derived from nuclear weapons testing (DeVries and Holzer, 2019).

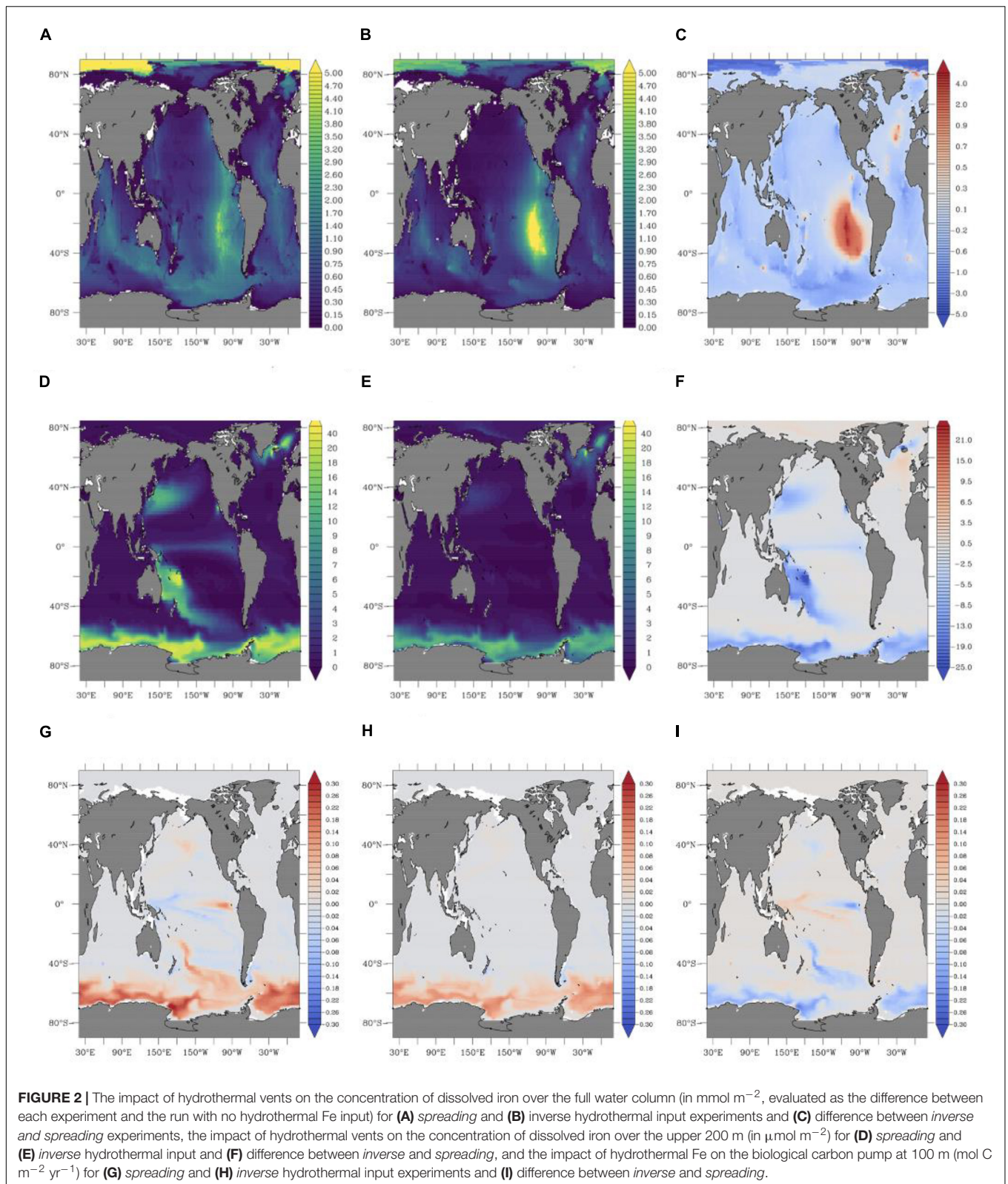
Anomalies in dFe due to hydrothermal Fe are calculated by comparing the dFe field from our model under either the *spreading* or *inverse* experiments to the *control* simulation with no hydrothermal Fe input. Calculated in this way, full depth integrated hydrothermal Fe signals largely follow the differences in hydrothermal Fe input between the two scenarios (Figures 2A,B), with the *inverse* experiment exhibiting a strong increase in dFe adjacent to the SEPR and locally south of the Azores along the northern mid Atlantic ridge. Relative to the *spreading* input, the *inverse* experiment causes persistent and widespread declines elsewhere, notably along the Southern ridge systems, throughout the Indian Ocean and southern mid Atlantic Ridge (Figure 2C). Turning to the upper 200 m, the hydrothermal

Fe signals that have made their way toward the ocean surface mixed layer can be isolated. Here, the overall pattern of the hydrothermal Fe anomaly is consistent between the two helium input scenarios, due to the identical circulation scheme used for these experiments and the well-known ventilation of <sup>3</sup>He into the Southern Ocean (Figures 2D,E). However, despite having the same total hydrothermal Fe supply as the *spreading* experiment, spatial differences in the *inverse* experiment cause a 4–5 fold reduction in the contribution of hydrothermal dFe in the upper 200 m (Figure 2F). The major differences between the two scenarios is now strongly localised in the Southern Ocean, where a large fraction of the hydrothermal Fe signal has been eliminated. Similarly, the Tonga Arc and Lau basin show no hydrothermal Fe signal under the *inverse* experiment, in contrast to local observations (Guieu et al., 2018). The difference in strength of the Fe anomaly between the depth integrated and 0–200 m inventories for both experiments reflects the substantial losses of hydrothermal Fe in the ocean interior due to scavenging discussed in early modelling efforts (Tagliabue et al., 2010).

### Impact of Hydrothermal Fe Supply Scenarios on Carbon Cycling

Anomalies in export production due to hydrothermal Fe closely follow the differences in 0–200 m dFe associated with hydrothermal supply. The *spreading* input experiment displays positive carbon export anomalies linked to hydrothermal Fe predominantly in the Southern Ocean, but with some smaller hotspots around the Lau basin (Cohen et al., 2021), north Pacific (Jenkins et al., 2020), and equatorial Pacific regions [Figure 2G, as in previous studies (Resing et al., 2015; Tagliabue and Resing, 2016)]. Small negative anomalies in export production arise due to downstream major nutrient deficits. Under the *inverse* input experiment, positive carbon export anomalies are restricted only to the Southern Ocean (Figure 2H). In line with the changes in the upper 200 m dFe signals, the Southern Ocean carbon export signal associated with hydrothermal Fe declines substantially during the *inverse* experiment (Figure 2I).





In the *spreading* input experiment, hydrothermal Fe stimulates export production by  $3.84 \text{ Tmol C yr}^{-1}$  south of  $40^\circ\text{S}$ , relative to a simulation with no hydrothermal Fe input [as in

prior work (Tagliabue and Resing, 2016)]. The contribution of hydrothermal Fe is reduced by over a third (36%) to  $2.45 \text{ Tmol C yr}^{-1}$  in the *inverse* input experiment. When changes to the

spatial distribution and supply of total hydrothermal Fe supply are accounted for in the *inverseR* experiment, the hydrothermal iron impact on Southern Ocean export production reduces by 73%, to  $1.06 \text{ Tmol C yr}^{-1}$ . Thus, the redistribution of hydrothermal Fe input away from the Southern ridges in the *inverse* input experiment causes a significant reduction in the assumed impact of hydrothermal Fe on Southern Ocean export production that is amplified when proposed adjustments to both the spatial distribution and magnitude of Fe inputs (Roshan et al., 2020) are accounted for. Overall, despite using a different circulation model and a more complete global Fe and C cycling model, we agree with Roshan et al. (2020) that there is negligible impact of hydrothermal Fe on the export production that supports the Southern Ocean biological carbon pump when the hydrothermal Fe input is parameterised based on  $^3\text{He}$  inverse modelling. Our experiments go further though, and also indicate that this difference is primarily due to the geographic distribution of hydrothermal Fe inputs along the global mid-ocean ridge crest, rather than being simply due to the overall magnitude of hydrothermal Fe supply between studies (as both the *spreading* and *inverse* experiments have the exact same total hydrothermal Fe supply).

## Constraints on Hydrothermal Fe Supply Scenarios From Southern Ocean Observations

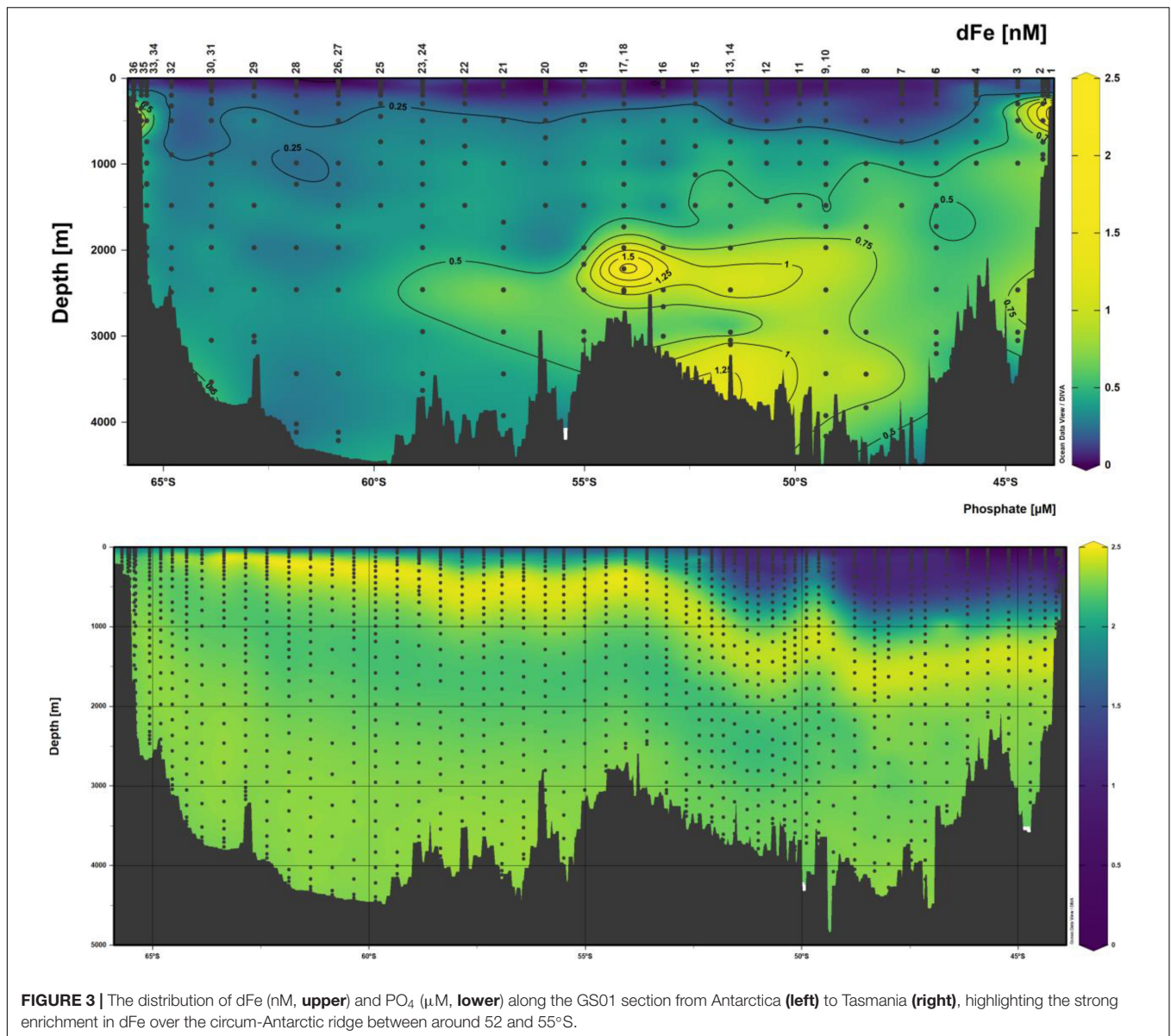
The *inverse*  $^3\text{He}$  input field has been shown to improve the reproduction of ocean  $^3\text{He}$  measurements (DeVries and Holzer, 2019), but the spatial redistribution of  $^3\text{He}$  inputs leads to the hydrothermal Fe anomaly reaching the upper ocean to be much reduced. As differences in the dFe anomalies around the circum-Antarctic ridges drive the majority of the Southern Ocean biological carbon pump signal associated with hydrothermal Fe, they provide the best observational constraints on different hydrothermal Fe input scenarios (Tagliabue and Resing, 2016). The GEOTRACES section cruise GS01 is the first full depth Southern Ocean section cruise to occupy meridional stations across the circum-Antarctic ridge between Hobart (Tasmania) and Antarctica. In the deep ocean (below 1,000 m depth), the dFe observations from the GS01 section are relatively uniform north and south of the circum-Antarctic ridge, located at around  $50\text{--}55^\circ\text{S}$  (Figure 3). The low deep-ocean values typical of the Southern Ocean endmember of around 0.4 nM and the slightly higher values closer to Tasmania of around 0.6 nM are similar to previous work in the region (Sedwick et al., 2008; Bowie et al., 2009). Most striking is the clear hotspot of dFe exceeding 1 nM above the circum-Antarctic ridge system that is well resolved across multiple stations and depths (Figure 3), and consistent with the observed abyssal dissolved manganese (dMn) distributions above and north and south of the ridge system (Latour et al., 2021).

Comparing the dFe fields from the *spreading* or *inverse* experiments to the available data shows that only *spreading* input experiment is able to reproduce the observed level of dFe enrichment above Southern Ocean ridges. We binned the GS01 observations onto the same vertical grid as the model

to ensure an appropriate comparison (Figures 4A,B). In the *spreading* experiment, the model reproduces the hotspot of dFe over the ridge observed during GS01 (Figures 4B,C) and displays a correlation coefficient of 0.63 along the entire GS01 abyssal ocean dataset (deeper than 1,000 m, Figure 4E). In contrast, the *inverse* experiment produces no discernible dFe signal above the ridge (Figure 4D) and has a  $\sim 3$ -fold lower correlation of 0.26 (Figure 4F). The correlation coefficient drops markedly to  $-0.24$  in the *inverseR* experiment, when we apply the optimised Fe/He ratio of Roshan et al. (2020) and the spatial distribution of  $^3\text{He}$  inputs from the *inverse* input, indicating anti correlation between the model and observations. Without any hydrothermal Fe input, the model becomes even more strongly anti-correlated with the GS01 observations ( $R = -0.47$ ), indicating the importance of significant hydrothermal Fe supply from Southern Ocean ridges in reproducing Southern Ocean dFe observations first advanced in earlier work (Tagliabue et al., 2010). Overall, this suggests that the greater impact of hydrothermal Fe on the biological carbon pump from the *spreading* experiment is more consistent with dFe observations.

## What Is the Residence Time for Hydrothermal Fe?

The residence time of hydrothermal Fe, relative to its ultimate removal by scavenging, is a key component governing its longevity and potential surface water ventilation. Observations from the GP16 section in the east Pacific using different tracers suggest that the hydrothermal iron emitted from the southern East Pacific Rise had a residence time of a few tens of years (Kipp et al., 2018; Anderson, 2020). This is lower than that implied from the quasi-conservative behaviour of iron, with respect to helium, observed during the 50–75 years transport of waters westward from the ridge crest (Resing et al., 2015; Fitzsimmons et al., 2017). Iron cycle modelling based solely on representing a pool of hydrothermal Fe and the *inverse* Fe boundary forcing suggests that the residence time of hydrothermal Fe was  $30 \pm 10$  years, implying little opportunity for surface ventilation (Roshan et al., 2020). In our modelling exercise, we can derive the residence time for hydrothermal Fe, relative to removal by scavenging, using the dFe anomaly with respect to the simulation with no hydrothermal Fe supply and the magnitude of the hydrothermal dFe boundary forcing appropriate for each experiment. The total hydrothermal iron inventory south of  $55^\circ\text{S}$  is 25 and 12 Gmol Fe (for the *spreading* and *inverse* experiments, respectively) or 250 and 210 Gmol Fe globally (for the *spreading* and *inverse* experiments, respectively). The companion Fe inputs are 1.1 and  $0.4 \text{ Gmol Fe yr}^{-1}$  in the Southern Ocean (for the *spreading* and *inverse* experiments, respectively) and  $10 \text{ Gmol yr}^{-1}$  globally for both scenarios. This results in hydrothermal Fe residence times of 22 and 34 years in the Southern Ocean (for the *spreading* and *inverse* inputs, respectively) or 25 and 21 years globally (for the *spreading* and *inverse* inputs, respectively). In our model, dFe gets stabilised due to interactions with ligands, alongside colloidal and scavenging interactions with the particle pool. The residence times derived are at the lower end of those previously proposed, yet we find hydrothermal Fe maintains a strong contribution to

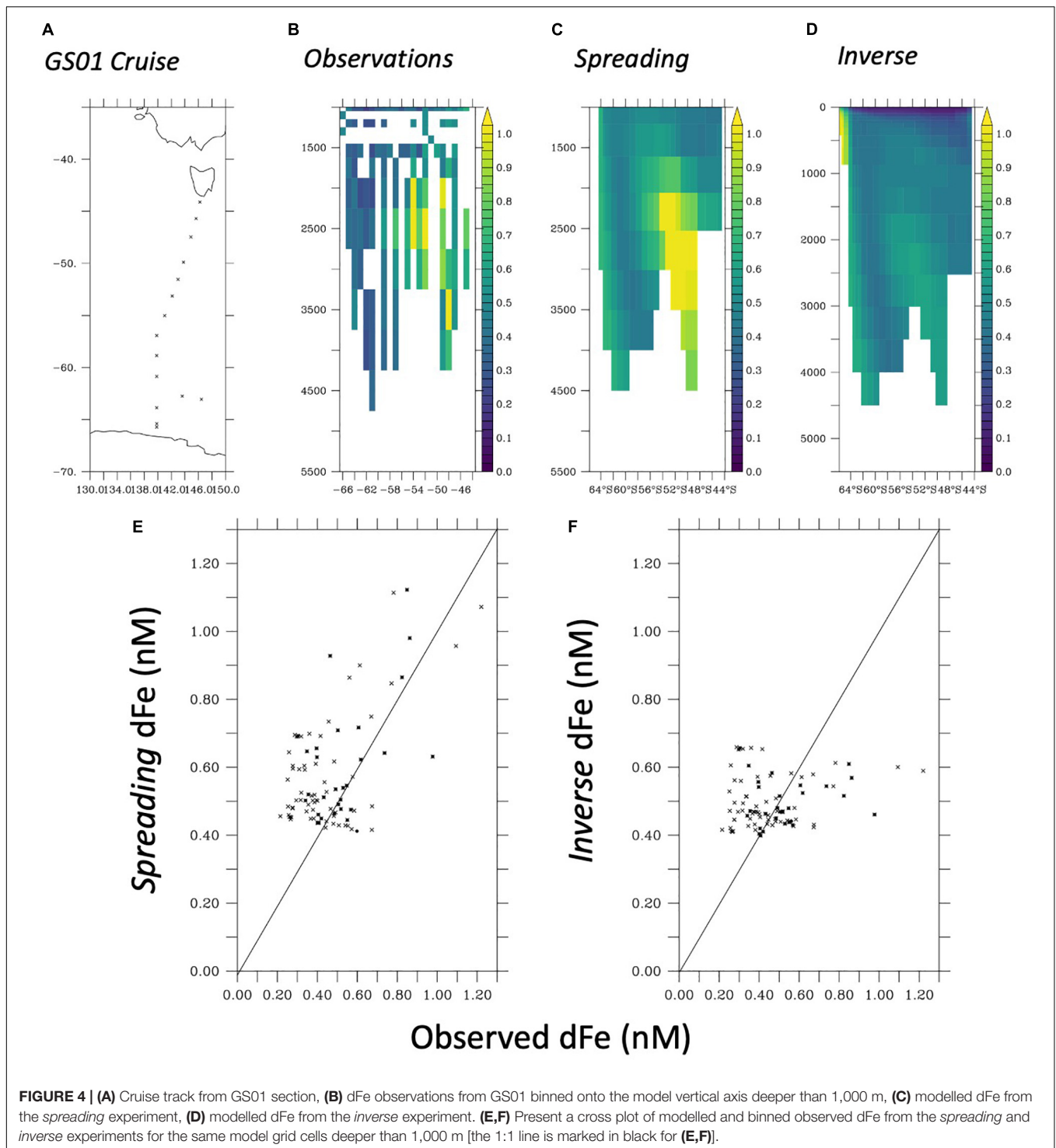


the export production that drives the Southern Ocean biological carbon pump. These results re-affirm the importance of Southern Ocean ridges (Tagliabue and Resing, 2016) as the critical factor governing hydrothermal Fe impacts on the carbon cycle, since only they can ventilate iron on sufficiently rapid timescales before hydrothermal Fe is removed by scavenging. Finally, our findings suggest that while hydrothermal vents outside of surface ventilation and mixing hotspots are important for the interior ocean Fe cycle, they are unlikely to affect the upper ocean significantly (unless they are present at shallow depths).

## WIDER IMPLICATIONS

Our findings suggest that trapping of Fe in the ocean interior by reversible scavenging is of secondary importance to the

geographic distribution of hydrothermal Fe supply, relative to ocean mixing regimes, in regulating the impact on the carbon cycle. Until now, modelling efforts have focussed on mid ocean ridge spreading systems in the Southern Ocean (e.g., **Figures 1A,B**), which neglects other sites of hydrothermal activity and iron supply. For instance, the Scotia Sea in the south Atlantic hosts a range of back arc and arc volcano sites that are notable iron sources (Hawkes et al., 2013, 2014) but are not yet accounted for in Fe cycle modelling efforts. Similarly, in the Indian sector, shallow venting from the active volcanoes around the Heard and McDonald Islands supplies Fe (Holmes et al., 2020) further south than the mid ocean ridge system. Finally, hydrothermal sites in the Bransfield Strait have been discovered (Klinkhammer et al., 2001), with Fe supply from the hydrothermal sediments inferred (Aquilina et al., 2014). It is clear that updated model hydrothermal sources above and



beyond those associated with mid-ocean ridges and moving beyond simple linkages with He will be important in addressing regional impacts on Fe cycling, especially in the Atlantic sector of the Southern Ocean.

While our ability to represent hydrothermal Fe will be helped by more complete datasets concerning inputs, the impact on the Southern Ocean carbon cycle requires a more holistic

consideration. Hydrothermal vents are not the only Fe source in the region, with important roles for margin sediments, sea ice, icebergs and melting glaciers, as well as aeolian deposition (from South America, Australia and southern Africa, alongside the dry valleys further south) (Boyd and Ellwood, 2010; Bhattachan et al., 2015; Tagliabue et al., 2017). The role for hydrothermal Fe operates alongside these other sources, which can end up

amplifying or dampening the carbon cycle impact in model assessments where the full range of iron sources are represented (Tagliabue et al., 2010). Spatially, hydrothermal supply is focussed on regions of deep water ventilation in the Antarctic sector (Figure 2), which overlaps most with sources associated with melting sea ice and transport of margin Fe from the Antarctic continental shelf (Boyd et al., 2012). This “Fe supply” mosaic will be important in attributing measured dFe signals to hydrothermalism (Schine et al., 2021). Progress on the Fe supply from hydrothermal vents alone will still leave outstanding questions regarding Fe supply from other sources.

The effective impact of Fe from Southern Ocean hydrothermal vents is regulated by the physical processes shaping the distribution, magnitude and timescales for deep ocean ventilation. Our study suggests that the residence time for hydrothermal Fe is on the order of a few tens of years, which requires upper ocean ventilation to be sufficiently rapid. The conservative hydrothermal tracer  $^3\text{He}$  has been estimated to emerge in Southern Ocean surface waters within  $99 \pm 18$  years (Jenkins, 2020), similar to the median re-exposure timescale from the deep Southern Ocean calculated from data constrained ocean physical models (DeVries and Holzer, 2019; Weber, 2020). Estimates from particle tracking models at higher spatial resolution suggest more rapid ventilation timescales of around 20 years, which slow to many decades in coarser resolution configurations (Tamsitt et al., 2017; Drake et al., 2018). Overall, ventilation timescales on the order of a few decades are compatible with a relatively short residence time for hydrothermal Fe. Ventilation of ridge associated signals may also be assisted if the topographic interaction promotes diapycnal transfer onto lighter isopycnals, which will then ventilate more rapidly (Sokolov and Rintoul, 2007). More focussed work on ocean mixing around Southern Ocean ridge systems over different space scales, alongside more process-based constraints on the rates and timescales of Fe removal, are necessary for improved insight.

## CONCLUSION

Combining ocean model experiments with new observations of dFe from the deep Southern Ocean, we find that the hydrothermal supply of Fe in the Southern Ocean is not well constrained by the spatial distribution of  $^3\text{He}$  inputs. This supports an important role of hydrothermal Fe in shaping upper ocean biological activity and export production in the Southern Ocean and the regional biological carbon pump. Due to the primary role played by hydrothermal Fe input along Southern Ocean ridges, the residence time of a few tens of years for hydrothermal Fe, relative to scavenging removal, estimated here is compatible with the expected physical mixing timescales in the region. Future work that expands the representation of

hydrothermal activity in the Southern Ocean beyond the mid ocean ridges will be important for refining ocean modelling and the carbon cycle impact. Expanded observational constraints on how the distribution and timescales of ocean physical mixing interface with ocean Fe cycling around Southern Ocean ridges will help develop more robust assessments of the fate and impact of hydrothermal Fe on the carbon cycle.

## DATA AVAILABILITY STATEMENT

The datasets presented in this study can be found in online repositories. The names of the repository/repositories and accession number(s) can be found below: <https://doi.org/10.5281/zenodo.5507411>.

## AUTHOR CONTRIBUTIONS

AT was designed the study, conducted all model experiments and their analysis, and led the writing of the manuscript with input from AB and JR. AB led the collection of dissolved iron data from the Southern Ocean. TH, PL, PM, MG-R, and KW participated in sample collection and analysis. All authors commented on the final draft and revisions.

## FUNDING

AT was supported by funding from NERC (NE/N009525/1). AB was supported by the Antarctic Climate and Ecosystems Cooperative Research Centre (ACE CRC) and Australian Research Council through the Future Fellowships Program (FT130100037). JR was funded by NOAA Earth-Ocean Interactions Program and Office of Ocean Exploration and Research and United States National Science Foundation OCE1756402.

## ACKNOWLEDGMENTS

We thank three reviewers for their comments that improved the manuscript. We also thank Tim DeVries (UCSB) for supplying the OCIM inverse model helium-3 input field. We wish to acknowledge the crew and officers of the Australian Marine National Facility Vessel RV Investigator for support at sea during the 2018 SR3 voyage (GS01) and also Morgane Perron, Christine Weldrick, Matthew Corkill, and Ashley Townsend for assisting with the sampling and sample processing. Data associated with this publication is available at: <https://doi.org/10.5281/zenodo.5507411>. This is PMEL contribution number 5293 and JISAO publication contribution 2021-1156.

## REFERENCES

- Anderson, R. F. (2020). GEOTRACES: Accelerating Research on the Marine Biogeochemical Cycles of Trace Elements and Their Isotopes. *Ann. Rev. Mar. Sci.* 12, 49–85. doi: 10.1146/annurev-marine-010318-095123
- Aquilina, A., Homoky, W. B., Hawkes, J. A., Lyons, T. W., and Mills, R. A. (2014). Hydrothermal sediments are a source of water column Fe and Mn in

- the Bransfield Strait, Antarctica. *Geochimica et Cosmochimica Acta* 137, 64–80. doi: 10.1016/j.gca.2014.04.003
- Ardyna, M., Lacour, L., Sergi, S., D'ovidio, F., Sallee, J. B., Rembauville, M., et al. (2019). Hydrothermal vents trigger massive phytoplankton blooms in the Southern Ocean. *Nat. Commun.* 10:2451. doi: 10.1038/s41467-019-09973-6
- Aumont, O., Ethé, C., Tagliabue, A., Bopp, L., and Gehlen, M. (2015). PISCES-v2: an ocean biogeochemical model for carbon and ecosystem studies. *Geosci. Mod. Develop.* 8, 2465–2513. doi: 10.5194/gmd-8-2465-2015
- Bhattachan, A., Wang, L., Miller, M. F., Licht, K. J., and D'odorico, P. (2015). Antarctica's Dry Valleys: a potential source of soluble iron to the Southern Ocean? *Geophys. Res. Lett.* 42, 1912–1918. doi: 10.1002/2015gl063419
- Bianchi, D., Sarmiento, J. L., Gnanadesikan, A., Key, R. M., Schlosser, P., and Newton, R. (2010). Low helium flux from the mantle inferred from simulations of oceanic helium isotope data. *Earth Planet. Sci. Lett.* 297, 379–386.
- Bowie, A. R., Lannuzel, D., Remenyi, T. A., Wagener, T., Lam, P. J., Boyd, P. W., et al. (2009). Biogeochemical iron budgets of the Southern Ocean south of Australia: decoupling of iron and nutrient cycles in the subantarctic zone by the summertime supply. *Glob. Biogeochem. Cycles* 23:4034.
- Boyd, P. W., Arrigo, K. R., Strzeppek, R., and Van Dijken, G. L. (2012). Mapping phytoplankton iron utilization: Insights into Southern Ocean supply mechanisms. *J. Geophys. Res.* 117:C06009.
- Boyd, P. W., and Ellwood, M. J. (2010). The biogeochemical cycle of iron in the ocean. *Nat. Geosci.* 3, 675–682.
- Cohen, N. R., Noble, A. E., Moran, D. M., Mcilvin, M. R., Goepfert, T. J., Hawco, N. J., et al. (2021). Hydrothermal trace metal release and microbial metabolism in the northeastern Lau Basin of the South Pacific Ocean. *Biogeosciences* 18, 5397–5422.
- DeVries, T., and Holzer, M. (2019). Radiocarbon and Helium Isotope Constraints on Deep Ocean Ventilation and Mantle 3-He Sources. *J. Geophys. Res. Oceans* 124, 3036–3057. doi: 10.1029/2018jc014716
- Drake, H. F., Morrison, A. K., Griffies, S. M., Sarmiento, J. L., Weijer, W., and Gray, A. R. (2018). Lagrangian Timescales of Southern Ocean Upwelling in a Hierarchy of Model Resolutions. *Geophys. Res. Lett.* 45, 891–898. doi: 10.1002/2017gl076045
- Dutay, J. C., Jean-Baptiste, P., Campin, J. M., Ishida, A., Maier-Reimer, E., Matear, R. J., et al. (2004). Evaluation of OCMIP-2 ocean models' deep circulation with mantle helium-3. *J. Mar. Sys.* 48, 15–36.
- Farley, K. A., Maier-Reimer, E., Schlosser, P., and Broecker, W. S. (1995). Constraints on mantle<sup>3</sup>He fluxes and deep-sea circulation from an oceanic general circulation model. *J. Geophys. Res.: Solid Earth* 100, 3829–3839. doi: 10.1029/94jb02913
- Fitzsimmons, J. N., John, S. G., Marsay, C. M., Hoffman, C. L., German, C. R., and Sherrill, R. M. (2017). Iron persistence in a distal hydrothermal plume supported by dissolved–particulate exchange. *Nat. Geosci.* 10, 195–201. doi: 10.1038/ngeo2900
- German, C. R., Casciotti, K. A., Dutay, J. C., Heimbürger, L. E., Jenkins, W. J., Measures, C. I., et al. (2016). Hydrothermal impacts on trace element and isotope ocean biogeochemistry. *Philosophical Transactions of the Royal Society. Math. Phys. Eng. Sci.* 374:20160035. doi: 10.1098/rsta.2016.0035
- Guieu, C., Bonnet, S., Petrenko, A., Menkes, C., Chavagnac, V., Desboeufs, K., et al. (2018). Iron from a submarine source impacts the productive layer of the Western Tropical South Pacific (WTSP). *Sci. Rep.* 8:9075. doi: 10.1038/s41598-018-27407-z
- Hatta, M., Measures, C. I., Wu, J., Roshan, S., Fitzsimmons, J. N., Sedwick, P., et al. (2015). An overview of dissolved Fe and Mn distributions during the 2010–2011 U.S. *Top. Stud. Oceanogr.* 116, 117–129.
- Hawkes, J. A., Connelly, D. P., Gledhill, M., and Achterberg, E. P. (2013). The stabilisation and transportation of dissolved iron from high temperature hydrothermal vent systems. *Earth Planet. Sci. Lett.* 375, 280–290. doi: 10.1016/j.epsl.2013.05.047
- Hawkes, J. A., Connelly, D. P., Rijkenberg, M. J. A., and Achterberg, E. P. (2014). The importance of shallow hydrothermal island arc systems in ocean biogeochemistry. *Geophys. Res. Lett.* 41, 942–947. doi: 10.1073/pnas.2019021117
- Holmes, T. M., Wuttig, K., Chase, Z., Schallenberg, C., Merwe, P., Townsend, A. T., et al. (2020). Glacial and Hydrothermal Sources of Dissolved Iron (II) in Southern Ocean Waters Surrounding Heard and McDonald Islands. *J. Geophys. Res. Oceans* 125:e2020JC016286.
- Holzer, M., DeVries, T., Bianchi, D., Newton, R., Schlosser, P., and Winckler, G. (2017). Objective estimates of mantle <sup>3</sup>He in the ocean and implications for constraining the deep ocean circulation. *Earth Planet. Sci. Lett.* 458, 305–314. doi: 10.1016/j.epsl.2016.10.054
- Jenkins, W. J. (2020). Using Excess 3-He to Estimate Southern Ocean Upwelling Time Scales. *Geophys. Res. Lett.* 47, e2020GL087266.
- Jenkins, W. J., Hatta, M., Fitzsimmons, J. N., Schlitzer, R., Lanning, N. T., Shiller, A., et al. (2020). An intermediate-depth source of hydrothermal <sup>3</sup>He and dissolved iron in the North Pacific. *Earth Planet. Sci. Lett.* 539:116223.
- Jenkins, W. J., Lott, D. E., German, C. R., Cahill, K. L., Goudreau, J., and Longworth, B. (2018). The deep distributions of helium isotopes, radiocarbon, and noble gases along the U.S. GEOTRACES East Pacific Zonal Transect (GP16). *Mar. Chem.* 201, 167–182. doi: 10.1016/j.marchem.2017.03.009
- Jenkins, W. J., Lott, D. E., Longworth, B. E., Curtice, J. M., and Cahill, K. L. (2015). The distributions of helium isotopes and tritium along the U.S. GEOTRACES North Atlantic sections (GEOTRACES GAO3). *Deep Sea Res. Part II Top. Stud. Oceanogr.* 116, 21–28.
- Kipp, L. E., Sanial, V., Henderson, P. B., Van Beek, P., Reys, J.-L., Hammond, D. E., et al. (2018). Radium isotopes as tracers of hydrothermal inputs and neutrally buoyant plume dynamics in the deep ocean. *Mar. Chem.* 201, 51–65. doi: 10.1016/j.marchem.2017.06.011
- Klinkhammer, G. P., Chin, C. S., Keller, R. A., Dählmann, A., Sahling, H., Sarthou, G., et al. (2001). Discovery of new hydrothermal vent sites in Bransfield Strait, Antarctica. *Earth Planet. Sci. Lett.* 193, 395–407. doi: 10.1016/s0012-821x(01)00536-2
- Klunder, M. B., Bauch, D., Laan, P., De Baar, H. J. W., Van Heuven, S., and Ober, S. (2012). Dissolved iron in the Arctic shelf seas and surface waters of the central Arctic Ocean: Impact of Arctic river water and ice-melt. *J. Geophys. Res. Oceans* 117:18.
- Klunder, M. B., Laan, P., Middag, R., De Baar, H. J. W., and Van Ooijen, J. C. (2011). Dissolved iron in the Southern Ocean (Atlantic sector). *Deep Sea Research Part II Top. Stud. Oceanogr.* 58, 2678–2694. doi: 10.1016/j.dsr2.2010.10.042
- Latour, P., Wuttig, K., Van, Der Merwe, Holmes, T. M., Corkill, M., and Bowie, A. R. (2021). Manganese biogeochemistry in the Southern Ocean, from Tasmania to Antarctica. *Limnol. Oceanogr.* 66, 2547–2562.
- Nishioka, J., Obata, H., and Tsumune, D. (2013). Evidence of an extensive spread of hydrothermal dissolved iron in the Indian Ocean. *Earth Planet. Sci. Lett.* 361, 26–33.
- Resing, J. A., Sedwick, P. N., German, C. R., Jenkins, W. J., Moffett, J. W., Sohst, B. M., et al. (2015). Basin-scale transport of hydrothermal dissolved metals across the South Pacific Ocean. *Nature* 523, 200–203. doi: 10.1038/nature14577
- Rijkenberg, M. J., Middag, R., Laan, P., Gerringa, L. J., Van Aken, H. M., Schoemann, V., et al. (2014). The distribution of dissolved iron in the West Atlantic Ocean. *PLoS One* 9:e101323. doi: 10.1371/journal.pone.0101323
- Roshan, S., DeVries, T., Wu, J., John, S., and Weber, T. (2020). Reversible scavenging traps hydrothermal iron in the deep ocean. *Earth Planet. Sci. Lett.* 542:116297. doi: 10.1016/j.epsl.2020.116297
- Saito, M. A., Noble, A. E., Tagliabue, A., Goepfert, T. J., Lamborg, C. H., and Jenkins, W. J. (2013). Slow-spreading submarine ridges in the South Atlantic as a significant oceanic iron source. *Nat. Geosci.* 6, 775–779.
- Schine, C. M. S., Alderkamp, A. C., Van Dijken, G., Gerringa, L. J. A., Sergi, S., Laan, P., et al. (2021). Massive Southern Ocean phytoplankton bloom fed by iron of possible hydrothermal origin. *Nat. Commun.* 12:1211. doi: 10.1038/s41467-021-21339-5
- Schlitzer, R., Anderson, R. F., Dodas, E. M., Lohan, M., Geibert, W., Tagliabue, A., et al. (2018). The GEOTRACES Intermediate Data Product 2017. *Chem. Geol.* 493, 210–223. doi: 10.1073/pnas.1603107114
- Sedwick, P. N., Bowie, A. R., and Trull, T. W. (2008). Dissolved iron in the Australian sector of the Southern Ocean (CLIVAR SR3 section): meridional and seasonal trends. *Oceanogr. Res. Pap.* 55, 911–925. doi: 10.1016/j.dsr.2008.03.011
- Sokolov, S., and Rintoul, S. R. (2007). On the relationship between fronts of the Antarctic Circumpolar Current and surface chlorophyll concentrations in the Southern Ocean. *J. Geophys. Res.* 112:7030. doi: 10.1029/2006JC004072
- Tagliabue, A., Bopp, L., Dutay, J. C., Bowie, A. R., Chever, F., Jean-Baptiste, P., et al. (2010). Hydrothermal contribution to the oceanic dissolved iron inventory. *Nat. Geosci.* 3, 252–256.

- Tagliabue, A., Bowie, A. R., Boyd, P. W., Buck, K. N., Johnson, K. S., and Saito, M. A. (2017). The integral role of iron in ocean biogeochemistry. *Nature* 543, 51–59. doi: 10.1038/nature21058
- Tagliabue, A., and Resing, J. (2016). Impact of hydrothermalism on the ocean iron cycle. *Philos. Trans. Math. Phys. Eng. Sci.* 374:20150291. doi: 10.1098/rsta.2015.0291
- Tamsitt, V., Drake, H. F., Morrison, A. K., Talley, L. D., Dufour, C. O., Gray, A. R., et al. (2017). Spiraling pathways of global deep waters to the surface of the Southern Ocean. *Nat. Commun.* 8:172.
- Völker, C., and Tagliabue, A. (2015). Modeling organic iron-binding ligands in a three-dimensional biogeochemical ocean model. *Mar. Chem.* 173, 67–77.
- Weber, T. (2020). Southern Ocean Upwelling and the Marine Iron Cycle. *Geophys. Res. Lett.* 47:e2020GL090737.
- Wuttig, K., Townsend, A. T., Van Der Merwe, P., Gault-Ringold, M., Holmes, T., Schallenberg, C., et al. (2019). Critical evaluation of a seaFAST system for the analysis of trace metals in marine samples. *Talanta* 197, 653–668. doi: 10.1016/j.talanta.2019.01.047

**Conflict of Interest:** The authors declare that the research was conducted in the absence of any commercial or financial relationships that could be construed as a potential conflict of interest.

**Publisher's Note:** All claims expressed in this article are solely those of the authors and do not necessarily represent those of their affiliated organizations, or those of the publisher, the editors and the reviewers. Any product that may be evaluated in this article, or claim that may be made by its manufacturer, is not guaranteed or endorsed by the publisher.

Copyright © 2022 Tagliabue, Bowie, Holmes, Latour, van der Merwe, Gault-Ringold, Wuttig and Resing. This is an open-access article distributed under the terms of the Creative Commons Attribution License (CC BY). The use, distribution or reproduction in other forums is permitted, provided the original author(s) and the copyright owner(s) are credited and that the original publication in this journal is cited, in accordance with accepted academic practice. No use, distribution or reproduction is permitted which does not comply with these terms.